International Journal of Heat and Mass Transfer 52 (2009) 3564–3575

Contents lists available at ScienceDirect

International Journal of Heat and Mass Transfer

journal homepage: www.elsevier.com/locate/ijhmt

Optimization of water and air management systems for a passive direct methanol fuel cell

Gregory Jewett, Amir Faghri *, Bin Xiao

Department of Mechanical Engineering, University of Connecticut, 261 Glenbrook Road, Unit 2337, Storrs, CT 06169, USA

ARTICLE INFO

Article history:
Received 2 February 2009
Received in revised form 7 March 2009
Accepted 7 March 2009
Available online 16 April 2009

Keywords:
Direct methanol fuel cell
Optimization
Numerical simulation
Passive

ABSTRACT

A multi-phase, multi-component, thermal and transient model is applied to simulate the operation of a passive direct methanol fuel cell and optimize the design. The model takes into consideration the thermal effects and the variation of methanol concentration at the feeding reservoir above the fuel cell. Polarization and constant current cases are numerically simulated and compared with experiments for liquid feed concentration, membrane thickness, water management and air management systems. Parameters considered when determining an optimal design include power density, fuel utilization and energy efficiencies and water balance coefficients. An optimal liquid feed concentration is determined to be 2.0 mol kg^{-1}, which achieved a maximum power density of 21 mW cm^{-2} and a fuel utilization efficiency of 63.0%. An optimal design of a cell uses a thick membrane (Nafion 117) to reduce methanol crossover and two additional cathode GDLs to improve the water balance coefficient and efficiency of the cell. This combination results in a power density of 23.8 mW cm^{-2} and a water balance coefficient of −1.71. An air filter may also be added to improve the efficiency and water balance coefficient of the cell, however, a small loss in power density will also occur. Using an Oil Sorbents air filter the water balance coefficient is increased to −0.85, the fuel utilization efficiency is improved by 27.35% and the maximum power density decreased to 21.6 mW cm^{-2}.

1. Introduction

Direct methanol fuel cells (DMFCs) are being investigated for portable power sources due to their higher power density, instant recharging and smaller size than batteries. Two principle issues with the development of DMFCs are methanol crossover and slow kinetics of methanol electro-oxidation reactions. Methanol crossover is a process where methanol diffuses through the membrane without reacting, generating heat and reducing power. This problem can be limited by maintaining a low methanol concentration at the anode of the cell, which requires a water and air management system if pure methanol is to be used as fuel.

A DMFC is an electrochemical device that converts chemical energy stored in methanol into electrical energy via the following oxidation and reduction reactions:

$$\text{Anode}: CH_3OH + H_2O \rightarrow CO_2 + 6H^+ + 6e^- \quad (1)$$

$$\text{Cathode}: 6H^+ + 6e^- + 1.5O_2 \rightarrow 3H_2O \quad (2)$$

$$\text{Overall}: CH_3OH + 1.5O_2 \rightarrow CO_2 + 2H_2O \quad (3)$$

Kinetic modeling of these reactions has been performed by many different research groups (Meyers and Newman [1], Garcìa et al. [2], Birgersson et al. [3,4], Kulikovsky [5]).

Meyers approached this task by first establishing a framework to determine equilibrium conditions of species in the proton exchange membrane (Meyers and Newman [1]). Next, kinematic modeling of the electrochemical reactions and transport phenomena were described (Meyers and Newman [6]). The final subject of Meyers work was to model the performance of a DMFC and optimize the design based on constraints of material properties (Meyers and Newman [7]). Meyers's optimization concluded that the methanol concentration should be as low as possible to achieve higher fuel efficiency, better cathode performance and overall better performance. With this in mind, the membrane used should be as thin as mechanical considerations will allow. Also, the catalyst layer should have as high a specific surface area as possible over as thin a layer as possible for increasing the reaction rate without increasing the ohmic drop of the active layer.

Garcia et al. [2] developed a model which can predict methanol concentration profiles in the anode backing layer, catalyst layer and membrane as well as accounting for methanol crossover through the cell. The model is one dimensional, isothermal and single phase (liquid). The model accounts for electro-osmotic drag of water which is the primary form of water transport at high current

* Corresponding author. Tel.: +1 860 486 0419; fax: +1 860 486 0479.
E-mail address: faghri@engr.uconn.edu (A. Faghri).

0017-9310/$ - see front matter © 2009 Elsevier Ltd. All rights reserved.
doi:10.1016/j.ijheatmasstransfer.2009.03.006

Nomenclature

D_{ij}	binary diffusivity (m^2/s)
$D_{eff,ij}$	effective diffusivity of gas phase (m^2/s)
F	Faraday constant (C/mol)
h_{fg}	latent heat of vaporization (J/kg)
h_m	mass transfer coefficient (ms)
$\mathbf{I}$	current density (A/m^2)
$\mathbf{I}_p$	proton current density ($proton/m^2s$)
$\mathbf{J}$	mass flux (kg/m^2s)
$J(s)$	Leverette function
k_{rg}	relative permeability of gas phase
k_{rl}	relative permeability of liquid phase
$\mathbf{K}$	permeability (m^{-2})
$\dot{m}'''$	mass source (kg/m^3s)
M_i	molecular weight of component i (kg/mol)
M_g	molecular weight of gas (kg/mol)
M_l	molecular weight of liquid (kg/mol)
n_d	electro-osmotic drag coeff. (mol/mol)
p_c	capillary pressure (Pa)
p_l	liquid pressure (Pa)
p_g	gas pressure (Pa)
t	time (s)
T	temperature (K)
s	liquid saturation
$\mathbf{V}_k$	velocity of phase k (m/s)
$\langle \mathbf{V}_k \rangle^k$	intrinsic phase velocity of phase k (m/s)

Greek symbols

ε	porosity
η	fuel consumption efficiency
λ	oxidation constant (mol/cm^3)
μ	viscosity (Ns/m^2)
θ	contact angle between liquid and solid (radians)
σ	surface tension (N/m)
σ_c	electrical conductivity of carbon phase ($\Omega^{-1}\ m^{-1}$)
σ_m	proton conductivity of membrane phase ($\Omega^{-1}\ m^{-1}$)
ρ	density (kg/m^3)
τ	tortuosity
$\omega_{g,i}$	mass fraction of gas (kg/kg)
$\omega_{l,i}$	mass fraction of liquid (kg/kg)

Subscripts

g	gas
i	component i
j	component j
l	liquid
m	membrane

densities. The model also considers the mixed potential at the cathode due to methanol crossover.

Baxter et al. [8] developed an isothermal, steady state model of the anode of a DMFC as well. Four components, water, methanol, carbon dioxide and hydrogen ions were transported in the anode. The study showed that the primary limiting factors of Pt:Ru catalysts are the kinetics of methanol oxidation and active surface area. The model could also predict the amount of methanol crossover through the membrane at different current densities as well as fuel flow rate to keep water-soluble levels of carbon dioxide in the anode pores.

There have been many models that have studied one dimensional and single phase fluid transport in a DMFC. However there are only a few models that are multi-dimensional and/or solve multi-phase flow. Taking into account all the effects of the components, phases, dimensions, thermal and transient operation is a critical task in developing a good model.

Kulikovsky [9] developed a two dimensional model based on mass and current conservations equations with a liquid methanol feed. The transport of methanol in the fuel channels was dominated by the pressure gradient, however in the active region diffusion transport was the dominating effect. The hydraulic permeability was determined to have a large effect on methanol crossover. If the hydraulic permeability of the backing layers were similar to that of the active layers and membrane, the electro-osmotic effect would create an inverse pressure gradient which reduces methanol crossover.

Ge and Liu [10] developed a single phase, three dimensional model which coupled traditional continuity, momentum and species conservation equations with electrochemical kinetics in the anode and cathode catalyst layers. A CFD finite volume approach was successfully used to simulate multi-component behavior in a DMFC. Methanol crossover, porous properties of the diffusion and catalyst layer, methanol flow rates and channel width are subsequently studied using the simulation.

Liu and Wang [11] also developed a three dimensional, two-phase model which considers in particular the transport of water and treats the catalyst layer explicitly instead of an interface without thickness. The basic model was extended from Wang and Wang [12] with a M^2 mixture model based on Wang and Cheng [13]. They determined that the anode flow field design and methanol concentration were two of the most important parameters for cell performance. They recommended a face feeding design which would provide a more uniform current density distribution and increase performance.

Wang and Wang [12] developed a two phase, multi-component model for a liquid feed DMFC using a two-phase mixture model (M^2). The model includes diffusion and convective effects for liquid and gas phases in the flow channels and backing layers. The model fully accounts for mixed potential effects that result from methanol oxidation due to crossover via diffusion, convection and electro-osmosis. Pasaogullari and Wang [14] also used the M^2 model, however they directly solved a flow equation for liquid saturation.

Rice and Faghri [15] developed a DMFC model which considered two dimensional, multi-phase, multi-component and transient effects. The evaporation and condensation rates were calculated to capture non-equilibrium effects between the phases. A passive liquid fuel delivery system which used multiple layers of porous media was modeled to demonstrate the feasibility of such a system. Rice and Faghri [16] added the energy equation to model ambient and cell temperature effects on cell performance.

Most passive portable systems are designed with the idea of a rechargeable container instead of a constant supply of fuel. Xiao and Faghri [17] modified the simulation in Rice and Faghri [15] for a liquid feed system which uses a reservoir for holding an initial amount of fuel or solution. This changes the transient effects when modeling the system because the solution concentration changes throughout the test instead of maintaining a constant concentration boundary condition. The constant voltage mode was also changed to a constant current density mode.

Jewett et al. [18] developed a water management system for a passive DMFC. Water was recovered from the cathode of the cell by adding water management layers to the cathode of the cell which had a micro-porous layer of 50 wt% PTFE on a carbon cloth. The micro-porous layer increased the hydraulic pressure at the cathode and forced water to pass back through the membrane to

the anode. Two water management layers were found to be adequate to maintain a water balance coefficient greater than zero for all current loadings. The air management system used various porous media as an air filter to block air borne particles from reaching the cathode. An Oil Sorbents filter was determined to be the best air filter based on its effects on cell performance, efficiency and water balance coefficient.

In this study, a numerical simulation, originally developed by Rice and Faghri [15–16] and later improved for transient operation by Xiao and Faghri [17], is used to predict the behavior of a liquid feed direct methanol fuel cell. Using the simulation, an optimized feed concentration and configurations for the water and air management systems and membrane thickness are then determined.

2. Background

2.1. Experiment

The geometry of the cell consists of multiple porous layers and a window frame structure with ribs, as described in Guo and Faghri [18,19]. The layers from anode to cathode are as follows: methanol concentration boundary layer, anode gas diffusion layer (GDL), anode catalyst layer, membrane, cathode catalyst layer, cathode gas diffusion layer, additional gas diffusion layers, air filter. The current collectors are very open structures and their effect on the fluids is considered to be negligible. The arrangement of these layers is shown in Fig. 1.

The water management system developed by Jewett et al. [18] consisted of additional gas diffusion layers between the cathode GDL and air filter. The additional GDLs were thicker than normal, 480 μm compared to 350 μm, and had a higher loading of 50 wt% PTFE applied to them, which were custom designed and provided by E-Tek. The additional gas diffusion layer was placed between the cathode gas diffusion layer and cathode current collector. This increased the diffusion length and the hydraulic pressure on the cathode side of the cell. The net effect was that water was pushed back across the membrane due to the pressure gradient at the cathode. Four cell configurations were tested: cell A with a Nafion 117 membrane and no additional GDL, cell B with a Nafion 117 membrane and one additional GDL, cell C with a Nafion 117 membrane and two additional GDLs and cell D which uses Nafion 112 in the MEA and two additional cathode GDLs, shown in Fig. 2.

The four air filters tested were Oil Sorbents (OS), ePTFE, porous polyethylene I (PPI) and porous polyethylene II (PPII). The filters have different properties as listed in Table 1, such as thickness, mean pore size (MPS) and porosity. The thickness of the filter plays a role in the trapping of particles as well as the amount of thermal insulation that the filter will provide. Each filter has a significant difference in thickness, with Oil Sorbents being the thickest at 4.77 mm, porous polyethylene I and II 2 mm and 1 mm, respectively, and ePTFE with a thickness of 250 μm. The MPS is important in determining the size of a particle that can penetrate the filter. Oil Sorbents has a MPS of 18.8 μm, porous polyethylene I has a MPS of 80–100 μm, porous polyethylene II has a MPS of 10–20 μm and ePTFE has a MPS of 0.5 μm. The porosity of the filter plays an important role in the flow of air as well as blocking particles from entering the cathode of the cell. Oil Sorbents has porosity around 90%, porous polyethylene I and II have porosities of 80% and 50%, respectively and ePTFE has a porosity of 40%.

Two types of tests were conducted on these cells: polarization and constant current. The polarization test is performed to confirm proper operation of the cell and determine the maximum power density and mass transport limitation. Three methanol solutions of 1.0, 3.0 and 5.0 mol kg^{-1} are tested for polarization. The test consists of reading the voltage of the cell as the current density is changed. The current density begins at 0.0 mA cm^{-2} and increased by 5 mA cm^{-2} until the cell voltage drops below 0.1 V. At each step the current density is held constant for 1 min and the average voltage is recorded.

The constant current experiments consisted of putting 10.0 g of 1.0, 3.0 and 5.0 mol kg^{-1} solutions in the cell reservoir and applying a constant current. The cell was allowed to operate in this manner until the voltage dropped below 0.1 V. At the end of the test the remaining solution was measured and the water balance coefficient, fuel utilization efficiency and energy efficiency were determined. The air management system was tested in a similar manner only with the addition of an air filter on the cathode side.

2.2. Physical model

The flow equations that were used in this formulation are continuity, momentum and species equations. The continuity equation for liquid and gas phases are given as

$$\frac{\partial}{\partial t}(\varepsilon s\rho_l) + \nabla\cdot(\varepsilon s\rho_l\langle\mathbf{V}_l\rangle^l) = \dot{m}_l''' \tag{1}$$

$$\frac{\partial}{\partial t}(\varepsilon(1-s)\rho_g) + \nabla\cdot(\varepsilon(1-s)\rho_g\langle\mathbf{V}_g\rangle^g) = \dot{m}_g''' \tag{2}$$

The capillary pressure describing the difference between the gas pressure and the liquid pressure in the fuel cell is

$$p_c = p_g - p_\ell = \sigma\cos\theta\left(\frac{\varepsilon}{k}\right)^{1/2} J(s) \tag{3}$$

$$J(s) = \begin{cases} 1.414(1-s) - 2.120(1-s)^2 + 1.263(1-s)^3 & \theta < \pi/2.0 \\ 1.411s - 2.120s^2 + 1.263s^3 & \theta \geq \pi/2.0 \end{cases} \tag{4}$$

These Eqs. (1)–(4) will apply to every region since they are all porous regions.

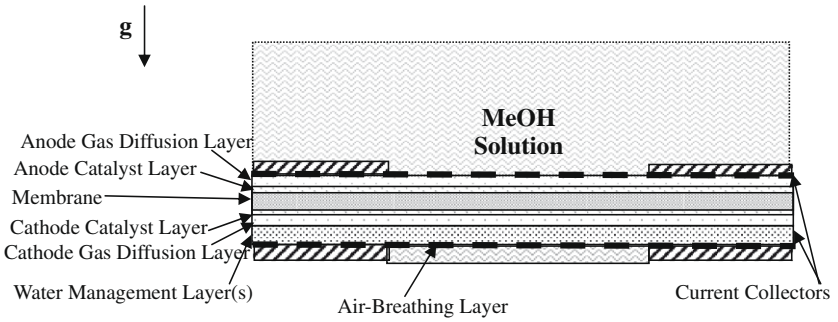

Fig. 1. Geometry of a passive DMFC polarization.

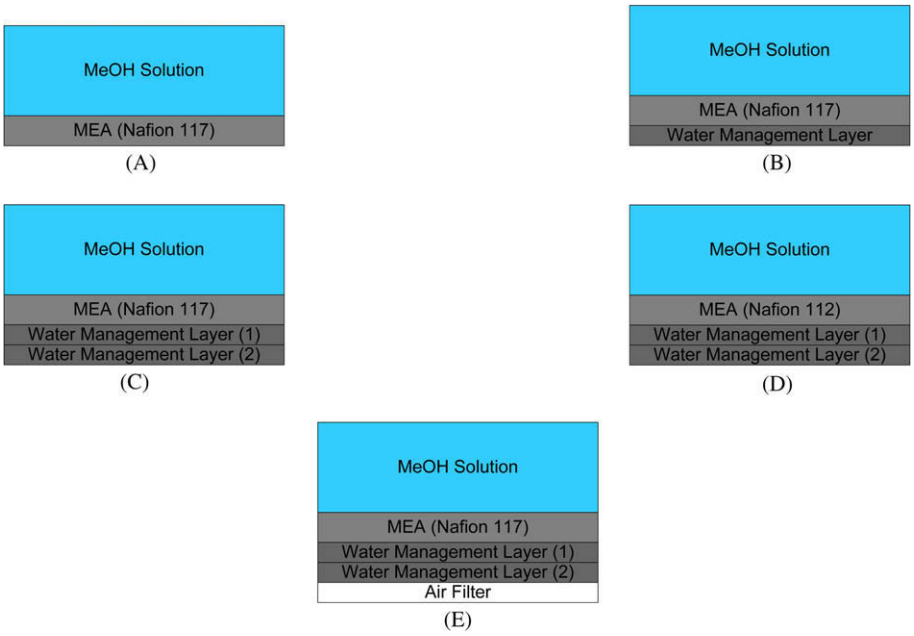

Fig. 2. Configurations for water management A, B, C and D and air management E for a passive DMFC.

Table 1
Material properties of DMFC layers.

Material	Thickness (μm)	Mean pore diameter (μm)	Porosity (%)	Permeability (m^2)	Manufacturer
Nafion 112	50.8		50	1×10^{-12}	Dupont
Nafion 117	177.8		50	1×10^{-12}	Dupont
Anode/cathode GDE	350		70	4×10^{-10}	E-Tek
Additional GDL	480	1.3	70	7.24×10^{-13}	E-Tek
SPC Oil Sorbents	4770	18.8	90	1.287×10^{-12}	Parmer Instrument Co.
Porous polyethylene I	2000	80-100	80	1.354×10^{-10}	Small Parts, Inc.
Porous polyethylene II	1000	10-20	65	6.773×10^{-11}	Small Parts, Inc.
ePTFE G110	250	0.5	40	4.464×10^{-13}	Saint Gorbain

The momentum equation for liquid and gas phases is based on Darcy's Law and given as

$$\varepsilon s\langle \mathbf{V}_l\rangle^l = -\frac{k_{rl}\mathbf{K}}{\mu_l}\nabla p_l + \frac{n_d M_l}{\rho_l}\frac{\mathbf{I}_p}{F} \tag{5}$$

$$\varepsilon(1-s)\langle \mathbf{V}_g\rangle^g = -\frac{k_{rg}\mathbf{K}}{\mu_g}\nabla p_g \tag{6}$$

The liquid and gas fluxes including the advection and diffusion term can be described by

$$\dot{m}''_{\ell,i} = \varepsilon s\rho_\ell\langle V_\ell\rangle^\ell - [\varepsilon s]^\tau \rho_\ell D_{1,12}\nabla\omega_{\ell,i} \tag{7}$$

$$\dot{m}_{g,i} = \varepsilon(1-s)\rho_g\langle V_g\rangle^g\omega_{g,i} - \sum_{j=1}^{N-1}[\varepsilon(1-s)]^\tau \rho_g D_{eff,i,j}\nabla\omega_{g,i} \tag{8}$$

The species equation in the liquid and gas phases are:

$$\frac{\partial}{\partial t}(\varepsilon s\rho_l\omega_{l,i}) + \nabla\cdot(\dot{\mathbf{m}}_{l,i}) = \dot{m}'''_{l,i} \tag{9}$$

$$\frac{\partial}{\partial t}(\varepsilon(1-s)\rho_g\omega_{g,i}) + \nabla\cdot(\dot{\mathbf{m}}_{g,i}) = \dot{m}'''_{g,i} \tag{10}$$

The methanol mass transportation from the feeding tank to the layer in the anode side is modeled by

$$\dot{m}''_{\ell,i} = \varepsilon s\rho_\ell\langle V_\ell\rangle^\ell M_{\ell,MeOH} + h_m(\omega_{feed,MeOH} - \omega_{\ell,MeOH}) \tag{11}$$

where h_m is the mass transfer coefficient and $\omega_{feed,MeOH}$ is the methanol fraction in the feeding tank.

A Stefan–Maxwell diffusion equation was used for the gas phases due to several components being present and for better accuracy.

$$\rho_g\nabla\omega_{g,i} = \sum_{j=1}^{N}\frac{M_g}{M_j}\frac{(\omega_{g,i}\mathbf{J}_{\mathbf{g,i}} - \omega_{\mathbf{g,i}}\mathbf{J}_{\mathbf{g,i}})}{D_{ij}} \tag{12}$$

The energy equation was used so that temperature effects could be included in the model and is given as:

$$\frac{\partial}{\partial t}(\varepsilon s\rho_l h_l + \varepsilon(1-s)\rho_g h_g + (1-\varepsilon)h_s) + \sum_i \nabla\cdot(\dot{\mathbf{m}}_{l,i}h_{l,i} + \dot{\mathbf{m}}_{g,i}h_{g,i}) = \nabla\cdot(k_{eff}\nabla T) + +\nabla\cdot(\phi_m\sigma_m\nabla\phi_m) + \nabla\cdot(\phi_c\sigma_c\nabla\phi_c) \tag{13}$$

A Gauss–Siedel iteration method was used for solving the flow equations. Convergence of the simulation was not done using residuals as it was found that residuals could even out, but a difference of 15% in results could still occur. Instead, randomly selected cells were monitored and when the cells' values changed by less than 0.1% from the previous iteration for 50 iterations, it was said to have converged.

2.3. Optimization procedure

The first step was to verify that the numerical simulation can predict experimental results. The first step to do this was by comparison of the polarization curves. The polarization curves were

found by scanning current, starting from 0 mA cm^{-2} and incrementally increasing by 5 mA cm^{-2} until the corresponding cell voltage is less than 0.1 V. Three different methanol concentrations of 1.0, 3.0 and 5.0 mol kg^{-1} were used for comparison with experimental data.

The optimization for methanol concentration was done using both polarization curves and transient simulations. The transient simulation was based on the experiments described in Jewett et al. [18]. A 10.0 g methanol solution was placed in the anode reservoir and a constant current was applied to the cell. The cell was allowed to operate until the cell voltage dropped below 0.1 V. The fuel and energy efficiency were calculated based on the amount of methanol used for useful power. The maximum power density and fuel efficiency were multiplied together and comparing the resulting number gave an effective means of determining the optimal concentration.

The optimization of the membrane thickness was performed in a similar manner as the concentration optimization. The thickness of the membrane was changed to 50.8 μm, 127 μm and 177.8 μm for Nafion 112, Nafion 115 and Nafion 117, respectively. The cell was allowed to operate at constant current until the cell voltage dropped below 0.1 V. The fuel and energy efficiency were calculated similarly to the concentration cases and the polarization curves were also found to find the maximum power density. The optimal design should have a high power density and efficient operation.

To optimize the water and air management systems, each configuration was modeled using the optimal concentration and membrane thickness. The three configurations simulated were (A) no additional cathode GDLs, (B) one additional cathode GDL and (C) two additional cathode GDLs, Fig. 2. The cell was modeled for polarization and constant current experiments. The water balance

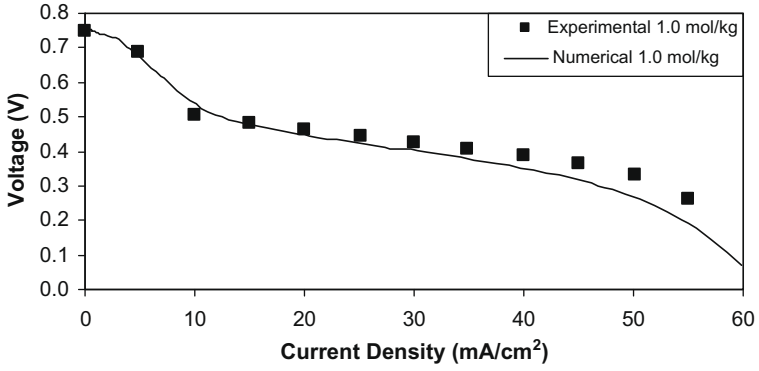

(a)

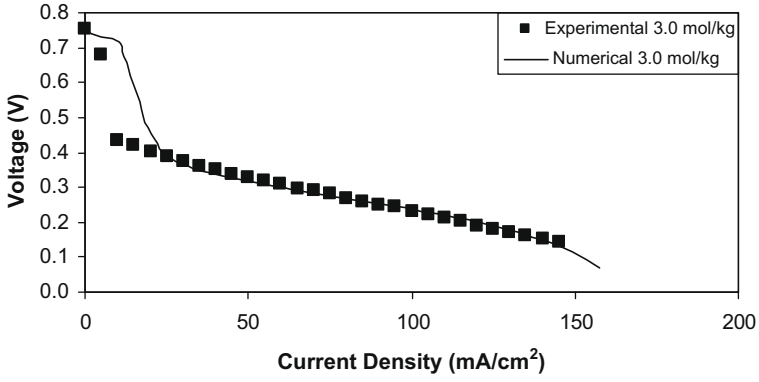

(b)

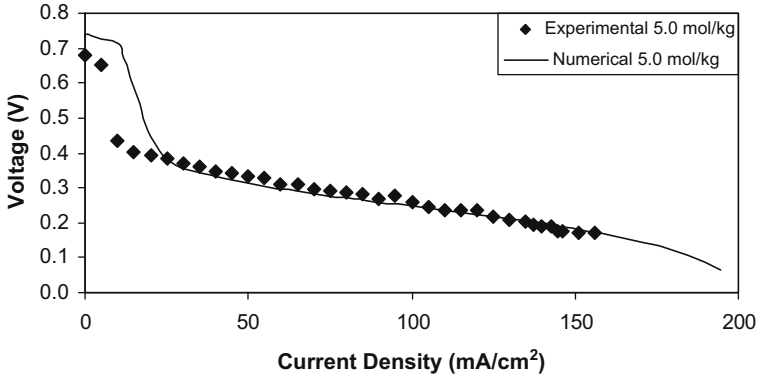

(c)

Fig. 3. Polarization comparison between experimental and numerical results for (a) 1.0 M, (b) 3.0 M and (c) 5.0 M solutions.

coefficient, power density and fuel and energy efficiencies were calculated to determine the best configuration.

The air management system was also optimized using the same procedure as the water management system. The air filter layer properties such as thickness, porosity and permeability were changed to match the four filters used in Jewett et al. [18]. The water balance coefficient, power density and fuel and energy efficiencies were calculated to determine the best air filter.

3. Results and discussion

The optimization procedure was carried out in multiple steps starting with calibration of the numerical simulation, then moving on to optimization of feed concentration, membrane thickness, water management system, and finally, air management system. Parameters used to define the optimization include the power density, water balance coefficient, fuel utilization efficiency and energy efficiency.

The water balance coefficient is defined as the ratio of water used to methanol used in moles [18]. This is normalized by subtracting the ratio from the two molecules generated during the reaction,

$$W_{BC} = 2 - \frac{\text{Water used (mol)}}{\text{Methanol used (mol)}} \tag{14}$$

Defining the water balance coefficient in this manner allows for quick recognition of the state of water in a cell. If the water balance coefficient is negative, then the cell is losing too much water. If the water balance coefficient is positive then the cell is recovering water from the cathode. If the water balance coeffi-

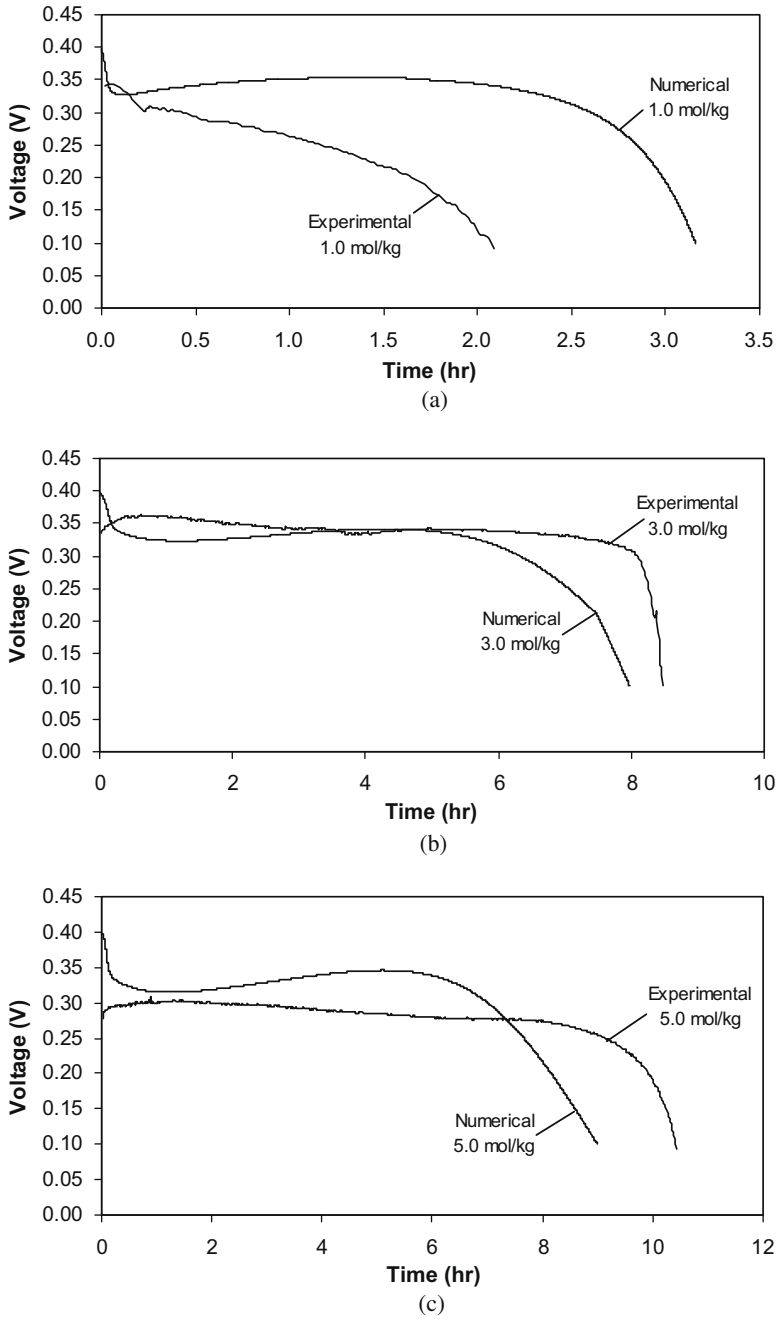

Fig. 4. Transient comparison between experimental and numerical results for (a) 1.0 mol kg^{-1}, (b) 3.0 mol kg^{-1} and (c) 5.0 mol kg^{-1} solutions.

cient is zero, then the cell is operating in water neutral conditions where the water lost from the cell exactly equals the water generated from the reaction. The goal is to achieve a water balance coefficient that is equal to or greater than zero.

The fuel utilization efficiency is defined as the amount of fuel used for useful energy divided by the total amount of fuel consumed Liu et al. [20].

$$\eta_{fuel} = \frac{\int j_{MeOH} dt}{(m_i C_i - m_f C_f) M_{MeOH}} \tag{15}$$

$$j_{MeOH} = \frac{I M_{MeOH}}{6F} \tag{16}$$

The energy efficiency is defined as the amount of energy produced divided by the theoretical amount of energy that could be produced.

$$\eta_{energy} = \frac{\int IV(t) dt}{(m_i C_i - m_f C_f) LHV} \tag{17}$$

where $V(t)$ is the voltage and LHV is the lower heating value of methanol, $LHV_{MeOH} = 638.1$ kJ mol^{-1} .

3.1. Calibration

Calibration of the simulation is done by modeling a polarization curve and comparing the simulation data with experimental results. The parameters that are changed to predict the results are

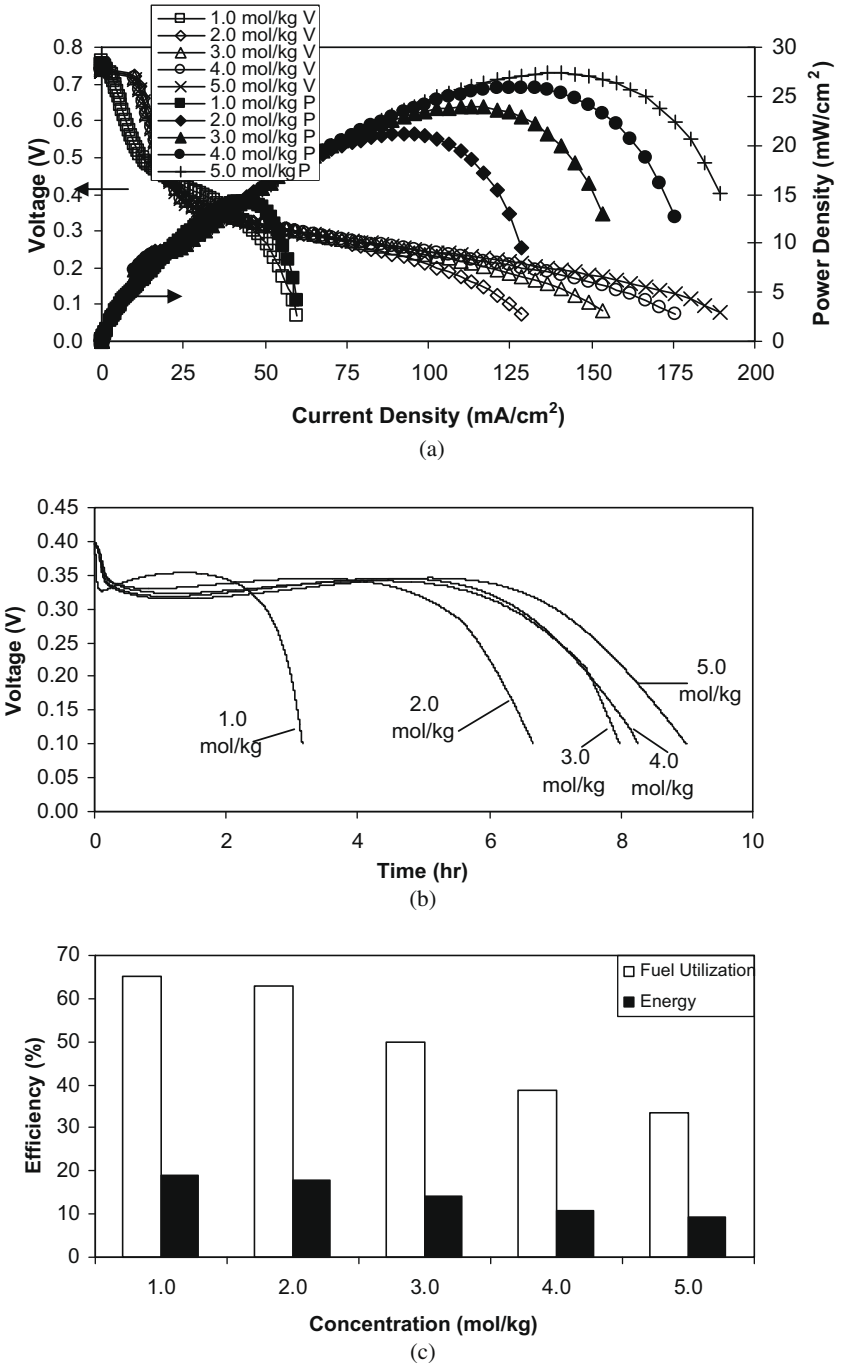

Fig. 5. Optimization of methanol concentration results (a) polarization comparison, (b) voltage vs. time and (c) fuel and energy efficiency.

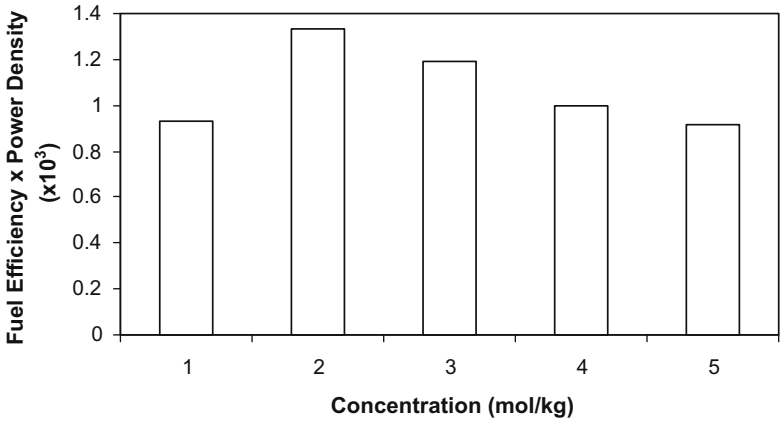

Fig. 6. Fuel utilization efficiency multiplied with power density for different methanol concentrations.

the anode and cathode transfer coefficients. These are part of the anode and cathode reaction equations and change the shape of the polarization curves.

A comparison of numerical and experimental results for 1.0, 3.0 and 5.0 mol kg^{-1} solutions are shown in Fig. 3. The anode transfer coefficient was set at 0.33 and the cathode transfer coefficient was set at 0.8. The case tested was cell A, shown in Fig. 2. The numerical results show the three distinct regions of a polarization curve, activation region, ohmic loss region and mass transport limitation region. The experimental polarization curves are stopped at about 0.1 V to protect the cells. This is why the numerical results extend past the experimental data. The numerical results match well with the experimental results, especially through the ohmic loss region. The 3.0 mol kg^{-1} and 5.0 mol kg^{-1} cases have a slightly larger activation region and higher starting voltages than their experimental counterparts, however, this could be due to methanol crossover causing mixed potentials at the start of the experimental polarization tests.

Comparisons of the experimental and numerical results for a constant current transient case are shown in Fig. 4. In Fig. 4a, the numerical results predict an operation time that exceeds the experimental case by about 1 h. This is caused by the simulation predicting a much lower methanol concentration at the end of the test – 0.117 mol kg^{-1} compared to the experimentally determined concentration of 0.25 mol kg^{-1} for a constant current of 0.3 A. In Fig. 4b and c, however, the numerical results predict shorter operation times than the experimental data despite having a lower concentration of methanol at the end of their tests. The difference here is caused by the increase in methanol crossover as the concentration is increased. The numerical simulation predicts a greater rate of methanol crossover through the cell, which results in shorter operation times. The important trend to note is that as the concentration is increased the operation time of the cell is increased which corresponds with experimental trends.

3.2. Concentration

Polarization curves were modeled using configuration A for five concentrations ranging from 1.0 mol kg^{-1} to 5.0 mol kg^{-1}. A comparison of the polarization curves for the concentrations is shown in Fig. 5a. The low concentration solution, 1.0 mol kg^{-1} only reached a maximum power density of about 16 mW cm^{-2}. As the concentration increased, the maximum power density increased as well; up to 27 mW cm^{-2}. The higher concentrations could also support higher current densities, over 175 mA cm^{-2}, than the low concentration solutions, 60 mA cm^{-2}, due to their increased mass transport limitation.

Transient cases were modeled for the same methanol concentrations. The cells were modeled at a constant current of 0.3 A until the cell voltage dropped below 0.1 V. The ambient conditions were 20 °C and 50% relative humidity. In Fig. 5b, the voltage of the cells throughout the tests can be seen. The voltage of the cell drops from the OCV as the current is applied at the very beginning. The voltage slowly rises as the temperature of the cell increases from the reaction. The mass transfer limitation occurs near the end of the test as the concentration of the solution becomes low, which results in the rapid decrease of cell voltage. High concentration solutions tend to have longer operation times as there is more solution that can be used during the course of testing. However, as the concentration increases, the operation time of the cell tends to increase more slowly. This is due to increased methanol crossover effects. As the concentration increases, the methanol crossover will increase, which reduces the operation time of a cell.

The efficiency of the cell using different concentration is shown in Fig. 5c. The highest fuel and energy efficiency is achieved using 1.0 mol kg^{-1} solutions. The efficiency decreases as the concentration increases and this is also due to methanol crossover. Methanol crossover is diffusion driven and as the concentration increases, so will the crossover of methanol. Therefore, using the lowest concentration possible will results in the highest fuel utilization and energy efficiency, however, to achieve high power density, a higher concentration solution should be used.

The power density and fuel utilization efficiency were multiplied together then divided by 1000 to determine the optimal methanol concentration on a reasonable scale, Fig. 6. An optimal concentration to use for the cell is about 2.0 mol kg^{-1} since it has a good power density of 21 mW cm^{-2} and good fuel utilization and energy efficiency, 63.0% and 17.8%, respectively.

3.3. Membrane thickness

The thickness of the membrane was changed next to simulate the effects of three different membranes, Nafion 112, 115 and 117. Polarization tests show that a thin membrane, Nafion 112, has a low power density due to methanol crossover causing a mixed potential, Fig. 7a. As the thickness is increased, the maximum power density of the cell is increased. This is again caused by a decrease in methanol crossover as the thickness of the membrane is increased. Since methanol crossover is diffusion driven, an increase in the diffusion length will decrease the amount of methanol that can crossover and cause a mixed potential.

Constant current testing was performed for the three membranes, Fig. 7b. The thicker membranes, Nafion 115 and 117, have much better sustainability than the thin membrane, again due to methanol crossover. Thin membranes will have significantly more methanol crossover than thicker membranes, which will result in a much shorter operation time with the same initial amount of fuel. Accordingly, the efficiency of the cell will be much worse with a thinner membrane due to methanol crossover, Fig. 7c. Nafion 117 has fuel utilization efficiency about 9% greater than that of Nafion 112 as well as an energy density 5.6% greater than that of Nafion 112 when modeling the cell at a constant current of 0.3 A.

The optimal membrane for these passive DMFCs is Nafion 117 because of its thickness, which significantly reduces the amount of methanol crossover. This increases the maximum power density of the cell as well as its operation time, fuel utilization and energy efficiencies.

3.4. Water management

An additional layer was added to the simulation to determine the effects and optimize the water management system. Three cases were simulated using this new numerical simulation: Cell A, B and C. Cell A was simulated by setting the layer's thickness to zero and setting the thickness of the other two cells to 0.48 mm and 0.96 mm.

The polarization curves show that as water management layers are added, the performance of the cell increases significantly, Fig. 8a. In experimental testing the difference between cells' per-

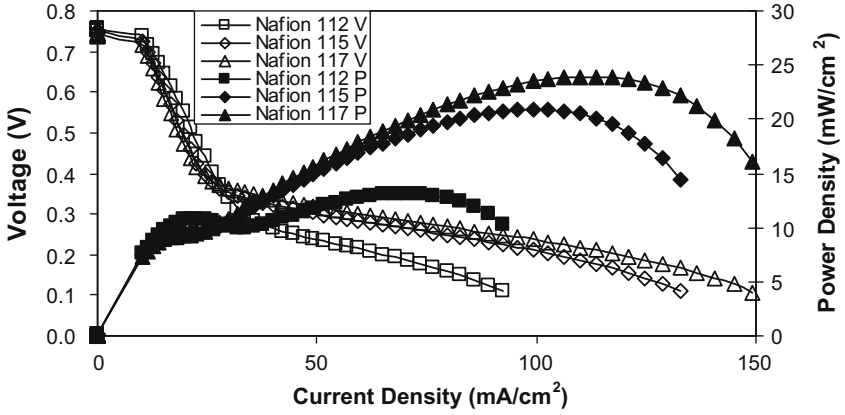

(a)

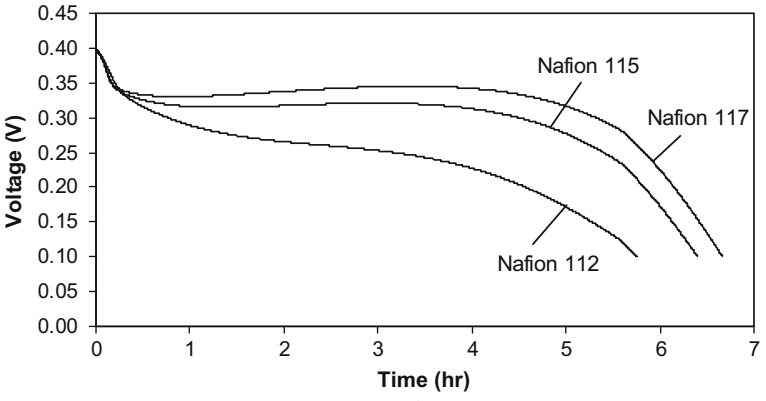

(b)

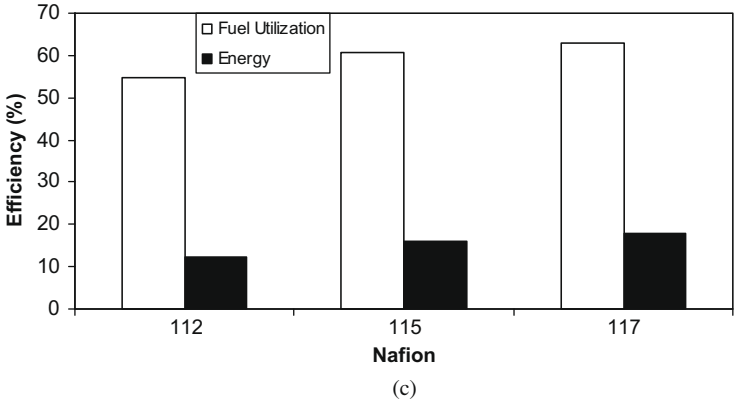

(c)

Fig. 7. Optimization of membrane thickness results (a) polarization comparison, (b) voltage vs. time and (c) fuel and energy efficiency.

formance was very small, typically less than a 2–3 mW cm^{-2}. The large difference in power density in the numerical simulation comes from the increased amount of air at the cathode. By increasing the water management layer thickness, the amount of air that can come into contact with the cathode also increases in the simulation. This results in the large increase in power density found in the simulation.

The transient cases show that as water management layers are added, the operation time of the cell increases, Fig. 8b. This coincides with experimental tests and is due to more water being recovered. By losing less water, the concentration at the anode stays lower than cases without water management layers, which reduces methanol crossover, increases operation time of the cells and results in higher efficiencies. Water balance coefficients were calculated for cases A, B and C as −3.63, −2.20 and −1.71, respectively. While these water balance coefficients are less than zero, they still show an improvement as water management layers are added. It is also observed that the addition of one water management layer has a significant impact on the water balance, a change of 1.43, however the addition of a second water management layer has a slightly reduced impact of 0.49. This trend also matches experimental data from Jewett et al. [18]. The best configuration for water management based on these numerical simulations would be to have two additional water management layers for performance, efficiency and water balance.

3.5. Air management

An air filter was added to the cathode side of the cell as shown in Fig. 2E. The filter needs to be able to block harmful particles while allowing sufficient air to pass through to the cathode. Four materials were tested, Oil Sorbents, ePTFE, porous polyethylene I (PPI) and porous polyethylene II (PPII) and their properties are given in Table 1.

Polarization curves were modeled for the cell with each air filter. As can be seen in Fig. 9a, there is very little difference in the performance of each cell. The maximum power density ranges from 21.1 to 21.6 mW cm^{-2} for all four cells. The maximum power density, 21.6 mW cm^{-2}, was achieved using the Oil Sorbents filter. This is less than the cell modeled without a filter, however, which reached a maximum power density of 23.8 mW cm^{-2}.

Transient modeling of the cell at a constant current of 0.3 A was performed and the voltage with respect to time is plotted in Fig. 9b. Again, the cell with different filters shows very little difference in performance and operation time. The cell operates continuously for 13–14 h before dropping below 0.1 V. Oil Sorbents again achieves the longest operation time and thus the best efficiency of the four filters. Oil Sorbents also has the most beneficial effect on the water balance of the cell. A water balance coefficient of −0.85 was achieved for the cell with the Oil Sorbents filter, which is a significant increase from −1.71 from the cell without an air filter.

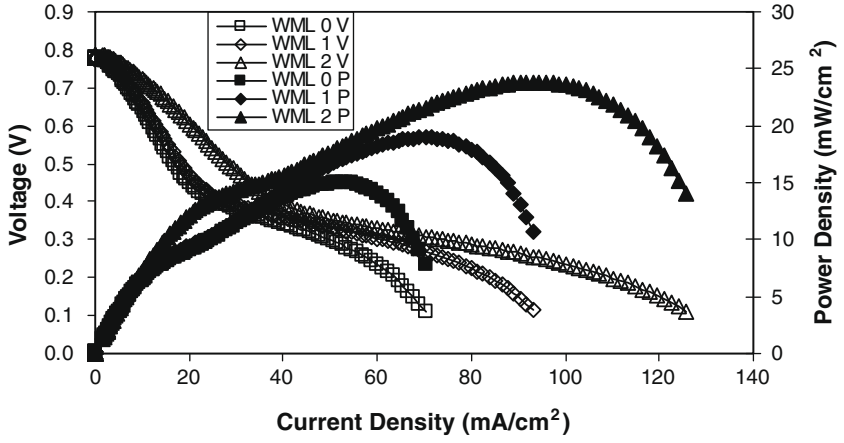

(a)

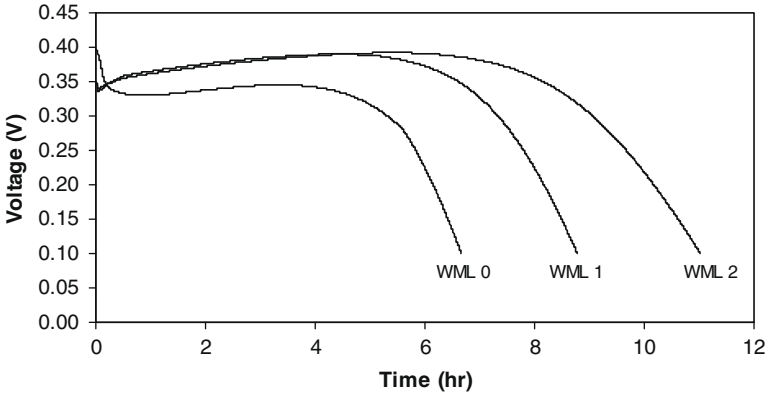

(b)

Fig. 8. Optimization of water management system results (a) polarization comparison and (b) voltage vs. time.

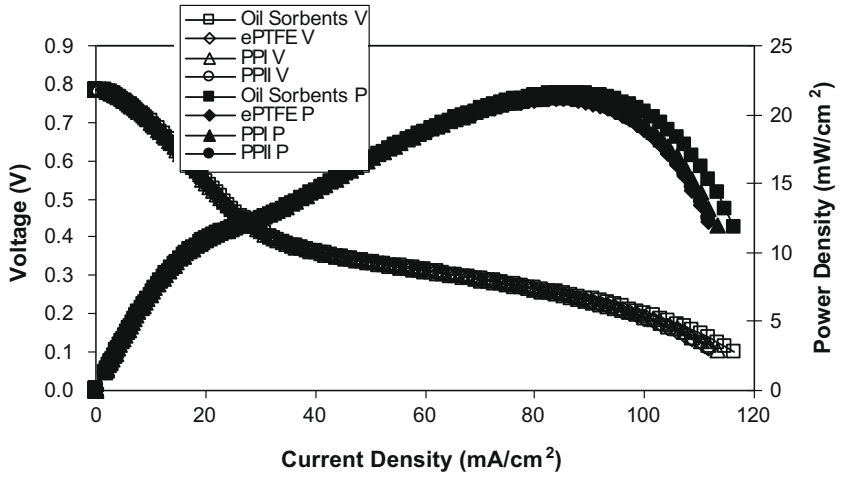

(a)

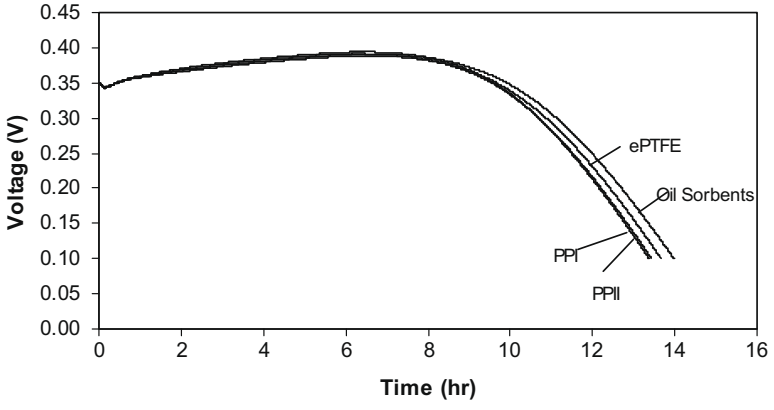

(b)

Fig. 9. Optimization of air management system results (a) polarization comparison and (b) voltage vs. time.

Based on the numerical results, an Oil Sorbents air filter provides the highest efficiency and water balance coefficient for the cell. The one drawback is that in using an air filter the power density of the cell is decreased by about 2 mW cm^{-2}.

4. Conclusion

Optimization of a passive direct methanol fuel cell was performed using a numerical simulation. High concentration solutions achieve high power densities, over 25 mW cm^{-2}, however low concentration solutions have much better efficiencies due to less methanol crossover. An optimal liquid feed concentration which balances power density and efficiency was determined to be 2.0 mol kg^{-1} with a combined power density and efficiency of 1.33×10^3. Thicker membranes such as Nafion 117 provide both higher power density, 23.9 mW cm^{-2} compared to 13.1 mW cm^{-2}, and greater efficiency, 63.01% compared to 54.89%, than thinner membranes such as Nafion 112 due to less methanol crossover.

A water management system which uses two additional cathode GDLs results in a greater water balance coefficient, −1.71, as well as increasing the power density and efficiency of the cell. An air management system which uses an Oil Sorbents air filter further improves the efficiency and water balance of the cell, −0.85. The addition of an air filter however also decreases the power density of the cell by about 2 mW cm^{-2}.

References

[1] J.P. Meyers, J. Newman, Simulation of the direct methanol fuel cell, J. Electrochem. Soc. 149 (2002) A710.
[2] B.L. Garcìa, V.A. Sethuraman, J.W. Weidner, R.E. White, R. Dougal, Mathematical model of a direct methanol fuel cell, J. Fuel Cell Sci. Technol. 1 (2004) 43.
[3] E. Birgersson, J. Nordlund, H. Ekström, M. Vynnycky, G. Lindbergh, Reduced two-dimensional one-phase model for analysis of the anode of a DMFC, J. Electrochem. Soc. 150 (2003) A1368.
[4] E. Birgersson, J. Nordlund, M. Vynnycky, C. Picard, G. Lindbergh, Reduced two-phase model for analysis of the anode of a DMFC, J. Electrochem. Soc. 151 (2004) A2157.
[5] A.A. Kulikovsky, On the nature of mixed potential in a DMFC, J. Electrochem. Soc. 152 (2005) A1121.
[6] J.P. Meyers, J. Newman, Simulation of the direct methanol fuel cell, J. Electrochem. Soc. 149 (2002) A718.
[7] J.P. Meyers, J. Newman, Simulation of the direct Methanol fuel cell, J. Electrochem. Soc. 149 (2002) A729.
[8] S.F. Baxter, V.S. Battaglia, R.E. White, Methanol fuel cell model: anode, J. Electrochem. Soc. 146 (1999) 437.
[9] A.A. Kulikovsky, Two-dimensional numerical modelling of a direct methanol fuel cell, J. Appl. Electrochem. 30 (2000) 1005–1014.
[10] J. Ge, H. Liu, A three-dimensional mathematical model for liquid-fed direct methanol fuel cells, J. Power Sources 160 (2006) 413–421.
[11] W. Liu, C.-Y. Wang, Three-dimensional simulations of liquid feed direct methanol fuel cells, J. Electrochem. Soc. 154 (2007) B352.
[12] Z.H. Wang, C.Y. Wang, Mathematical modeling of liquid-feed direct methanol fuel cells, J. Electrochem. Soc. 150 (2003) A508.
[13] C.Y. Wang, P. Cheng, Adv. Heat Transfer 30 (1997) 93.
[14] U. Pasaogullari, C.Y. Wang, Two-phase transport and the role of micro-porous layer in polymer electrolyte fuel cells, Electrochim. Acta 49 (2004) 4359–4369.

[15] J. Rice, A. Faghri, A. Transient, Multi-phase and multi-component model of a new passive DMFC, Int. J. Heat Mass Transfer 49 (2006) 4804–4820.
[16] J. Rice, A. Faghri, Thermal and startup characteristics of a miniature passive liquid feed DMFC system including continuous and discontinuous phase limitations, ASME J. Heat Transfer 130 (2008).
[17] B. Xiao, A. Faghri, Transient modeling and analysis of methanol transport and performance in a passive DMFC, Int. J. Heat Mass Transfer 51 (2008) 3127–3143.
[18] G. Jewett, Z. Guo, A. Faghri, Water and air management systems for a passive direct methanol fuel cell, J. Power Sources 168 (2007) 434–446.
[19] Z. Guo, A. Faghri, Development of planar air breathing direct methanol fuel cell stacks, J. Power Sources 160 (2006) 1183–1194.
[20] J.G. Liu, T.S. Zhao, Z.X. Liang, R. Chen, Effect of membrane thickness on the performance and efficiency of passive direct methanol fuel cells, J. Power Sources 153 (2006) 61–67.